GSI

GSI-Preprint-98-19
April 1998

BETA-DECAY OF ^{40}Ti AND ^{41}Ti AND IMPLICATION FOR SOLAR-NEUTRINO DETECTION

W. Liu, M. Hellström, R. Collatz, J. Benlliure, L. Chulkov, D. Cortina Gil, F. Farget, H. Grawe, Z. Hu, N. Iwasa, M. Pfützner, A. Piechaczek, R. Raabe, I. Reusen, E. Roeckl, G. Vancraeynest, A. Wöhr

Gesellschaft für Schwerionenforschung mbH
Planckstraße 1 • D-64291 Darmstadt • Germany
Postfach 11 05 52 • D-64220 Darmstadt • Germany

Beta–decay of ^{40}Ti and ^{41}Ti and implication for solar-neutrino detection

W. Liu[1*], M. Hellström[1], R. Collatz[1], J. Benlliure[1], L. Chulkov[2], D. Cortina Gil[1], F. Farget[1], H. Grawe[1], Z. Hu[1], N. Iwasa[1], M. Pfützner[1,3], A. Piechaczek[1], R. Raabe[4], I. Reusen[4], E. Roeckl[1], G. Vancraeynest[4], A. Wöhr[4]

[1] *Gesellschaft für Schwerionenforschung, D-64291 Darmstadt, Germany*

[2] *Kurchatov Institute, 123182 Moscow, Russian Federation*

[3] *Institute of Experimental Physics, University of Warsaw, PL-00681 Warsaw, Poland*

[4] *Institut voor Kern-en Stralingsfysika, Katholieke Universiteit, B-3030 Leuven, Belgium*

(March 26, 1998)

Abstract

The β-decay of ^{40}Ti and ^{41}Ti was studied by measuring the β-delayed proton- and γ-emission. The half-lives for ^{40}Ti and ^{41}Ti were determined to be 54(2) and 82(3) ms, respectively. The experimental β-decay strengths are compared with shell-model calculations and results from other measurements. The integrated Gamow-Teller strengths for ^{40}Ti and ^{41}Ti were found to be quenched, compared to the calculations, by factors of 0.79(3) and 0.93(3), respectively. Based on the experimental ^{40}Ti β-decay strength, the neutrino absorption cross-section and induced neutrino event rates for ^{40}Ar were determined to be $14.3(3)\times10^{-43}$ cm^2 and $9.4\pm0.2(\text{stat.})^{+1.3}_{-1.6}(\text{syst.})$ SNU, respec-

---

* Permanent address: China Institute of Atomic Energy, P.O. Box 275(60), Beijing 102413, P.R. China

tively.

23.40.-s, 23.50.+z, 27.40.+z, 96.60.Kx

I. INTRODUCTION

In the ICARUS detector [1], the energy and direction of electrons scattered by the incoming solar neutrinos as well as of electrons produced in the inverse β-decay $^{40}\mathrm{Ar}(\nu_e,e^-)^{40}\mathrm{K}$ can be measured in a large-volume liquid argon time-projection chamber. Since the inverse β-decay to the ^{40}K ground state is forbidden, each neutrino absorption is accompanied by γ-rays emitted from excited ^{40}K levels, which results in production of Compton electrons. In this way, the electron multiplicity distinguishes scattering and absorption events, making it possible to measure the ratio R between these two types of events. R is independent on the total neutrino flux impinging on a terrestrial detector whereas it depends significantly on possible neutrino oscillations. This is due to the fact that electrons can be scattered by electron neutrinos as well as by μ and τ neutrinos while the production of electrons via neutrino absorption is restricted to electron neutrinos only. Furthermore, quantitative information on the oscillation probability $\nu_e \rightarrow \nu_{\mu,\tau}$ can be obtained from the experimental R values.

In order to make the evaluation of ICARUS data reliable, the cross sections for the different interaction processes must be known very well. The scattering rates can be accurately calculated by using the standard electroweak theory [2] whereas the situation is more complicated for the case of neutrino absorption. While an accurate value for the Fermi transition strength $B(F)$ between the ^{40}Ar ground state and the isobaric analog state (IAS) in ^{40}K is given by the model-independent sum-rule [3], it is more difficult to determine the transition strengths $B(GT)$ for the individual allowed Gamow-Teller contributions to the neutrino-capture rate. In principle, the $B(GT)$ values for the inverse β-decay can be deduced by using shell-model theory, or from data measured for the zero-degree charge-exchange reaction $^{40}\mathrm{Ar(p,n)}^{40}\mathrm{K}$. However, as was shown recently, shell-model calculations fail in reproducing the $B(GT)$ distributions measured in the region around ^{40}Ca [4-7]. Furthermore, the proportionality of β-decay transition strengths and zero-degree (p,n) reaction rates has been questioned, because a comparison of the β-decay of ^{37}Ca with the $^{37}\mathrm{Cl(p,n)}^{37}\mathrm{Ar}$ mirror

reaction [4] shows differences that are probably not entirely due to isospin-violating effects [8,9]. Hence, a calibration of the neutrino absorption rate based on shell-model calculations or on (p,n)-reactions might jeopardize the quality of the ICARUS results.

An alternative possibility for calibrating the ^{40}Ar neutrino capture rate is to use, under the assumption of isospin symmetry, the $B(GT)$ values of the mirror β^+-decay of ^{40}Ti. In principle, the large energy release of the ^{40}Ti decay (Q_{EC} = 11680(160) keV [10]) enables one to extract all information that is relevant for the Gamow-Teller contributions to the rate of solar neutrinos absorbed by ^{40}Ar. In this context, we note that the efficiency calibration for the ^{37}Cl experiment has recently been achieved in a similar way by using the $B(GT)$ values measured in the β^+-decay of ^{37}Ca, see [7] for a recent review.

Another motivation for this study is to obtain data on high energy-release β^+-decay at the beginning of the *fp* shell similar to those available from recent experiments on the β^+-decays of ^{36}Ca [5], ^{37}Ca [6], and ^{38}Ca [11]. Such data are of interest for further clarification of the evident discrepancy between data from β^+-decay, charge-exchange reactions, and shell-model calculations. It is interesting to note that ^{40}Ti, together with $^{36-39}$Ca, are the only nuclei whose β^+-decays represent mirror transitions to (p,n) reactions on stable-isotope targets.

We performed a measurement of the ^{40}Ti β^+-decay which, prior to our work, had been investigated in only one experiment with severely limited statistics [12]. The latter measurement yielded only singles data of β^+-delayed protons whereas in our experiment proton-γ coincidences were measured. This information is indispensable in order to clarify whether the β^+-delayed proton emission populates the ground-state and/or excited states of ^{39}Ca. Furthermore, the decay of ^{41}Ti was studied in order to establish an energy calibration for the ^{40}Ti proton data and to improve, by detection of β^+-delayed γ-rays, the results of previous ^{41}Ti studies. A short communication of the ^{40}Ti data obtained in this work has already been published elsewhere [13], and similar work was published soon after [14]. The present paper summarizes the results of our refined data analysis and presents details of the experimental technique, the data analysis, and the determination of experimental $B(GT)$ values. The paper is structured as follows: Sect. II deals with the experimental set-up, Sect. III de-

scribes the data analysis, and Sect. IV contains the discussion of the decay strengths for ^{40}Ti and ^{41}Ti from this work in comparison with experimental and theoretical results obtained previously as well as the calculation for the ^{40}Ar neutrino absorption cross sections; Sect. V gives summary and outlook.

II. EXPERIMENTAL TECHNIQUES

A. Production of ^{40}Ti

A ^{58}Ni beam of 500-A MeV with an intensity of 1×10^{9} ions/s from the heavy-ion synchrotron SIS of GSI, Darmstadt, was used to produce ^{40}Ti by fragmentation reactions in a 4 g/cm^2 thick ^{9}Be target. The secondary ^{40}Ti beam was isotopically separated by using the projectile fragment separator FRS [15]. The FRS was operated with two degraders at the first and intermediate focal plane to achieve both a more narrow range profile and higher purity of the ^{40}Ti beam with respect to contaminating secondary beams, in particular β-delayed proton emitters such as ^{41}Ti. By inserting a degrader in the first focal plane, the ratio of ^{40}Ti to ^{41}Ti was improved from 10 to 100. The intensity of the ^{40}Ti beam at the final focus of the FRS amounted to about one atom per minute. During the experiment of 5 days, about 1.1×10^{4} ^{40}Ti ions were produced. The experimental setup is sketched in Fig. 1. The ^{40}Ti ions were identified by energy-loss (ΔE) and mass-to-charge ratio (A/q). ΔE was determined by means of a multiple sampling ionization chamber (MUSIC), and A/q by measurements of the time-of-flight (TOF) and the magnetic rigidity of the FRS. The TOF was determined by using two scintillation counters (SC) positioned at the intermediate (F_2) and final (F_4) focal planes, respectively, and corrected by the position information (X/Y) measured by means of two multi-wire proportional chambers (MWPC). Fig. 2 shows a scatter plot of events on a ΔE versus A/q plane.

B. Implantation and proton–γ detection

As shown in Fig. 1, the ^{40}Ti beam was collimated by a slit of ± 5 cm aperture in the dispersive dimension. The slit, in combination with the trigger signal derived from the implantation detector (see below), should in principle restricts the A/q values to a range between 1.75 and 1.89. However, due to the low-energy tail in the fragment energy distribution, many unexpected ions were also transmitted to the implantation detectors. Fortunately, the influence of other positron or β-delayed proton emitting contaminants was small, since the most intense products observed at F_4 were stable isotopes (see Fig. 2). Such contaminants were further rejected by a delayed-coincidence between the identified ^{40}Ti events and time-correlated decay events, as described in Sect. III. The ^{40}Ti beam was slowed down at F_4 from 240-A MeV to 60-A MeV by using a 0.7 g/cm^2 thick aluminum degrader. This measure was taken in order to shift the implantation profile to the center of the silicon detector stack consisting of eight 300 μm thick, 30 mm diameter silicon detectors. The three central counters were used to measure positrons and β-delayed protons, whereas the outer ones served as veto detectors to reject unwanted particles as described below. About 90 % of the ^{40}Ti ions arriving at F_4 were implanted in the central three counters. The measured range profile, shown in Fig. 3, has a full-width at half maximum of about 630 μm. The signals of each silicon detector, stemming from passage/implantation of heavy ions, or from positron or proton decays, were processed by a common pre-amplifier. Low- and high-gain main amplifiers were used to take the different energy ranges into account which were 100-1000 MeV and 0-10 MeV, respectively. A time generator allowed to record the arrival time of each event for the determination of the decay half-life.

An array of 11 large-volume Crystal Ball NaI detectors [16] were mounted close to the silicon detector stack to measure γ-rays emitted in the ^{40}Ti or ^{41}Ti decay processes. The NaI detectors were selected due to their higher photo-peak efficiencies compared to standard germanium detectors.

C. Energy and efficiency calibration of the detectors

The energy and efficiency calibration of the NaI array was obtained by using standard calibration sources. The photopeak efficiency was measured to be 15(2) % at 1.33 MeV, which is an order of magnitude higher than that obtained by using two large-volume germanium detectors in previous FRS experiments [7].

The proton-energy (E_p) calibration has to taken into account the pulse-height defect of the ^{39}Ca recoil atoms [17] and the line shifts caused by the summation between β-ray energy loss and proton signals. To address this problem, we performed the energy calibration of the silicon detectors by implanting the known β-delayed proton emitter ^{41}Ti [18] in the separate experiment, with the FRS being optimized for this isotope. The difference in the line-shifts occurring in the β-delayed proton spectra of ^{40}Ti and ^{41}Ti is negligible [19].

A first rough energy calibration of the silicon detectors was obtained by using an α source and a pulse generator. This calibration was then improved on the basis of the β-delayed proton spectrum of ^{41}Ti. The resultant uncertainty of E_p amounts to 10–15 keV for the major peaks. The detection efficiencies for the silicon detectors were determined from experimental data as well as from a Monte-Carlo simulation, as discussed below.

III. DATA ANALYSIS

A. Event selection

The delayed-coincidence technique, used in the off-line data analysis of the ^{40}Ti data, was based on a time window of 200 ms. This window was opened by a ^{40}Ti event, selected according to conditions with respect to ΔE and A/q (see Fig. 2), and closed by the subsequent decay event. In this way, decay events from positron and/or β-delayed proton emitters (e.g. ^{38}Ca, see Fig. 2) were rejected. The selected decay events contained proton and γ-ray energy information. The E_p spectra were generated by an anti-coincidence condition with the front and rear silicon counters in order to eliminate heavy ions which were stopped

in the first counter or penetrated through all of them. The proton events which were not completely stopped in a single detector were rejected by an anti-coincidence condition with adjacent counters. The identification of the stopping of ^{40}Ti ions in any of the three central detectors was also used to select only the decay signals that were recorded in the relevant counter. This condition rejected the β-background stemming from contaminants implanted in neighboring detectors. The analysis of the ^{41}Ti data was performed in a similar way, with the implantation-decay window being 300 ms.

B. Proton spectra

The proton energy spectra obtained from the three central silicon counters were used to extract the intensities of individual proton transitions (I_p). Figs. 4 and 5 show the ^{40}Ti and ^{41}Ti proton spectra, respectively. The I_p values of major peaks were determined by adding the contribution from the central part and from the low- and high-energy tails of the lines. The proton peak shape function used in this procedure was established by the major proton peaks as well as by a Monte-Carlo simulation. The I_p values of small peaks were obtained by simple integrations after subtraction of the background from fitted major peaks. A typical peak fitting procedure is shown in Fig. 6. For an E_p range above four MeV, the E_p and I_p values of small peaks have large uncertainties due to the poor counting statistics, the influence of the phase space factor, and the inferior full-energy detection efficiency described below.

To improve the energy resolution, a range selection method was applied. It consisted of selecting those events which correspond to ^{40}Ti atoms stopped in the central 100 μm thick layer of one of the three central silicon detectors. This was accomplished by comparing the measured residual energy of ^{40}Ti ions with range-energy relation [20]. As can be seen by comparing Figs. 4 and 7, the proton energy resolution was improved by this method from 100 keV to 70 keV at a proton energy of 3.7 MeV.

The I_p values were corrected for the full-energy detection efficiency. The latter quantity

was determined by selecting events recorded in coincidence between the adjacent counters. The experimental results obtained in this way are displayed in Fig. 8, in comparison with results from a Monte-Carlo simulation [21] based on the proton stopping power in silicon. To get the proton branching ratios (b_p) for individual proton transitions, the I_p values were normalized to the total number of implanted ^{40}Ti ions. The latter quantity was deduced from the ΔE versus A/q data displayed in Fig. 2, and corrected for the intensity loss due to secondary reactions in the energy degrader at F_4 (See Sect. II.B). This loss amounted to 13(3) %, which was determined experimentally by using the energy-loss and the residual energy measured for the heavy-ions in the silicon counters, as shown in Fig. 9. This result is in good agreement with an estimate of 10 %, based on systematics of fragmentation cross-sections [22]. The final E_p and b_p values for ^{40}Ti and ^{41}Ti, listed in Tables I and II, respectively, represent weighted averages based on the results from different detectors and range selection conditions. The sum of individual b_p values for ^{40}Ti and ^{41}Ti amounts to 101(5) and 104(5) %, respectively. The agreement of these results with a value of 100 % yields (i) an integral proof for the consistency of the corrections concerning intensity losses and proton full-energy efficiency, and (ii) a 1σ limit of order of 5 % for the branching ratio of *unobserved* β-delayed protons or γ-rays from the decay of ^{40}Ti and ^{41}Ti, respectively. Tables I and II compile the E_p and b_p results from this work compared to literature data for ^{40}Ti and ^{41}Ti, respectively.

C. Proton-γ coincidence data

The proton-γ coincidence data were used to identify proton emission from ^{40,41}Sc levels to excited states of ^{39,40}Ca. This information was used to deduce the β-branching ratios (b_β) from the experimental b_p values. The resulting b_β data for ^{40}Ti and ^{41}Ti are listed, together with the proton decay mode (p_0, p_1, p_2), in Tables III and IV. A typical proton-γ coincidence pattern is shown in Fig. 10. Fig. 11 displays the γ-ray spectra measured in coincidence with 1322 and 2167 keV protons. As can be seen from Figs. 10 and 11, there is

clear evidence for a proton transition between the 4365 keV isobaric analog state (IAS) in ^{40}Sc and the 2469 keV state in ^{39}Ca. A ratio of 12(3) % was found between the number of γ-gated events in the 1322 keV proton peak and the number of events observed for this peak in the ungated spectrum (see Fig. 4). This value is in good agreement with the calibrated NaI photopeak efficiency of 13(3) % at 2.5 MeV (see Sect. II.C). Correspondingly, the intensity of the 1322 keV proton line is assigned to a IAS→2469 keV transition. The remaining ^{40}Ti and ^{41}Ti proton-γ coincidence data were interpreted in a similar way.

Gamma-transitions in ^{40,41}Sc could in principle be searched for by demanding NaI events in coincidence with positrons, i.e. with low-energy signal derived from the silicon detectors. No such β-delayed γ-ray events were found. It is clear from Figs. 10 and 11, however, that there is only a small number of events just above the electronic threshold that could be candidates for positrons emitted in the decay of ^{40}Ti and ^{41}Ti, respectively. Therefore, our experiment is not very sensitive for recording of γ-transitions in ^{40}Sc or ^{41}Sc. The upper limit for the branching ratio for all β-delayed γ-rays is 5 % in both cases, as mentioned above.

D. Half-life determination

The distributions of time periods, elapsed between implantation and β-decay of ^{40}Ti and ^{41}Ti, were generated by the delayed-coincidence technique described in Sect. III.A. To suppress β-background from other nuclei, only events corresponding to E_p values larger than 1.5 MeV were used. Fig. 12 shows the time spectrum obtained for ^{40}Ti. The half-lives ($T_{1/2}$) of ^{40}Ti and ^{41} Ti, measured to be 54(2) and 82(3) ms, respectively, are compared with the results of other works in Table V. Good agreement within the experimental uncertainties is achieved for both nuclei.

E. Determination of β-decay strength

The β-decay strength functions $B(GT)$ and $B(F)$ were deduced by using the relation [6] $[B(F) + B(GT)]_i = 6127(9)s/ft_i$, with $t_i = T_{1/2}/b_{\beta i}$, and $f(Q_{EC} - E_x, Z)$ being the phase space factor in β-decay and E_x the excitation energy in the daughter nucleus. This evaluation was based on $T_{1/2}$ results from this work. As discussed by Trinder *et al.* [14], the Q_{EC} value of ^{40}Ti of 11680(160) keV from the literature [10] can be improved by applying the isobaric multiplet mass equation (IMME) and using the experimental excitation energy of the ^{40}Sc IAS state, measured by Trinder *et al.* [14] of 4365(8) keV as well as in this work of 4365(10) keV (see Table III). We followed the suggestion of Trinder *et al.* and used the revised ^{40}Ti Q_{EC} value of 11466(13) keV [14], to calculate the transition strengths for ^{40}Ti. The Q_{EC} value for β-decay of ^{41}Ti was taken to be 12932(40) keV from the mass compilation [10].

The $B(F)$ and $B(GT)$ values from this work are displayed in Fig. 13 and listed in Table III in comparison with results from the other recent β-decay measurement [14], a ^{40}Ar(p,n)^{40}K experiment [26], and a shell-model calculation [27]. Fig. 14 and Table IV show the corresponding results for ^{41}Ti.

IV. DISCUSSION

A. Decay strengths of ^{40}Ti

In this work, we are able to identify 18 new proton peaks compared with our previous analysis [13], and nine new proton peaks compared with Ref. [14]. This progress is due to the reduction of the β-background and the more detailed analysis of small proton peaks described in Sect. III.A. Five proton energy groups were assigned, according to the proton-γ coincidence data, to proton transitions to the 2169 keV state in the ^{39}Ca. The ratio between the IAS(^{40}Sc)$\rightarrow$2169keV(^{39}Ca) decay and the IAS(^{40}Sc)$\rightarrow$g.s.(^{39}Ca) transition is 17(3) %. The 951 keV proton peak was assigned to a transition to the 3026 keV $3/2^-$ state in ^{39}Ca.

even though the corresponding proton-γ coincidence relation was not observed. This non-observation can be explained by taking the intensity of the 951 keV proton peak and the NaI efficiency for 3026 keV γ-ray into account. Moreover, if one would assign this line to a transition to the ^{39}Ca ground state, the resulting ^{40}Sc excitation energy would not have a corresponding level in the mirror nucleus ^{40}K which has been extensively studied. The J^{π} assignment for ^{40}Sc levels populated by β-decay of ^{40}Ti are 1^{+}, except for the 1365 keV level which was identified as the IAS. The latter interpretation is based on the observed β-strength of 4.01(31), which agrees with the theoretical value of $\mid Z - N \mid = 4$ for a pure Fermi transition.

The integrated $B(GT)$ value is 5.84(39), which can be compared with the shell-model result of 5.62 [27], which was obtained by the free-nucleon GT operator quenched by a factor of 0.775. The latter value is in good agreement with the result of 0.79(3) obtained from a comparison of our experimental data with "unquenched" shell-model results. The integrated experimental $B(GT)$ above the IAS is 2.28(30), whereas the shell-model gives 3.33. In addition to this discrepancy, we note that the shell-model overestimates the excitation energies of the first two excited states of ^{40}Sc by roughly one MeV, as can be seen from Fig. 13; a similar difference in excitation energy was also observed for the ^{37}Ca decay [28]. To some extent these discrepancies result from the truncation in model space introduced in the shell-model calculation [29].

Excellent agreement is found between the present results and those obtained by Trinder *et al.* [14] up to a ^{40}Sc excitation energy of 5 MeV . At higher excitation energies, however, the GT strength from this work is more fragmented than that obtained by Trinder *et al.*. This discrepancy is not surprising as the statistics of our data (see Fig. 4) as well as of those obtained by Trinder *et al.* is too poor for proton energies above 5 MeV for an *unambiguous* decomposition into individual transitions. Our data agree with those of the (p,n) work [26]. The $B(GT)$ values for the sum of the first two states are in good agreement with present result. The difference in the ratio between these two states may due to the difference in the configuration mixing in ^{40}Sc and ^{40}K. Note that, due to detector response function (see

Sects. II.C and III.B) and the strong energy dependence of the phase-space factor in β-decay, our experiment was not very sensitive to be determination of β-strength above a ^{40}Sc excitation energy of 6 MeV. This is illustrated by the fact that a $B(GT)$ value of 0.1 for a ^{40}Sc level at 6.5 MeV corresponds to a b_β value of only 0.1 %, the corresponding proton line being characterized by a large width (FWHM about 150 keV) and a peak-to-total ratio below 50% (see Fig. 6).

The recent ^{40}Ti β-decay study of Trinder *et al.* [14] is characterized by better statistics and lower electronic thresholds of the silicon detectors compared to our work: the latter feature was used to improve the proton energy resolution by β-energy selection in neighboring detectors. Our work, however, profited from higher purity of the ^{40}Ti beam with respect to contaminating positron and β-delayed proton emitters, and from higher detection efficiency for γ-rays. The former effect reduced the probability of chance coincidences in the delayed-coincidence procedure, and resulted thus in purer proton energy and decay time distributions. We also used thinner silicon detectors (300 μm) than those used by Trinder *et al.* (500 μm), which reduced β-summing effects but decreased the full-energy detection efficiency. Furthermore, by using the information of the detector number where the ^{40}Ti ions were stopped, we obtained lower β-background. In summary, the two experiments are complementary, with the good agreement in the I_p results from both works being indeed remarkable.

B. Decay strengths of ^{41}Ti

On the basis of the proton-γ coincidence data, five transitions were assigned to populate the 3904 keV state in ^{40}Ca. Although there is reasonable overall agreement between our b_β results and those of previous works [18,23,24], substantial deviations remain for individual b_β values, in particular at high excitation energies. Correspondingly, our $B(GT)$ values are significantly larger at high excitation ^{41}Sc energies than those of Honkanen *et al.* [18] , as can be seen from Fig. 14. In evaluating this discrepancy, we note that the b_β results from

this work are based on the absolute counting of ^{41}Ti ions, whereas all the earlier experiments [18,23,24] simply nomalized the sum of the experimental I_p values to 100 %. Furthermore, proton-γ coincidence data have not been available previously. These experimental improvements are probably also responsible for the fact that three new ^{41}Sc levels of high excitation energy were identified in the present work.

The integrated $B(GT)$ strength of 5.6 for ^{41}Ti, determined by shell-model calculations [18], is larger than the values of 4.83(29) from this work. This most probably stems from the fact that no quenching factor was introduced in the calculation. As shown in Fig. 14, the $B(GT)$ prediction agrees with experiment with respect to the gross structure but overestimates the individual strengths at ^{40}Sc excitation energies of 4-6 MeV, and fails to reproduce the noticeable $B(GT)$ strengths at even higher excitation energy. The overall GT quenching was obtained to be 0.93(3).

C. Calculation of ^{40}Ar neutrino absorption cross-sections

The highest-lying ^{40}Sc level identified in this work has an excitation energy of 6426(30) keV, compared with the proton separation energy of 7582 keV [10] in the mirror nucleus ^{40}K. Therefore, the present experiment covers most of the strengths relevant to the ^{40}Ar neutrino capture process. Following the procedure suggested by Ormand *et al.* [27], we calculated the ^{40}Ar neutrino absorption rates, based on the experimental ^{40}Ti β-decay strength from this work and the updated solar neutrino flux of $6.6^{+0.9}_{-1.1} \times 10^6$ cm^{-2}s^{-1} [30]. In this calculation, we used the experimental ^{40}K excitation energies whenever possible; otherwise the ^{40}Sc excitation energies from this work were taken, as shown in Table III. The resultant neutrino absorption cross sections of ^{40}Ar and the neutrino induced event rates for the ICARUS detector are $13.8(6)\times10^{-43}$ cm^2 and $9.1\pm0.1(\mathrm{stat.})^{+1.3}_{-1.6}(\mathrm{syst.})$ SNU, respectively. The systematical uncertainty is related to the calculation of the solar neutrino flux [30]. As shown in Table VI, these results are in agreement with our previous evaluation [13], the data obtained by Trinder *et al.* [14], the results based on (p,n) work [26], and the shell-

model prediction [27]. However, the neutrino absorption cross-section from these sources is approximately four times higher than that calculated by Bahcall [2] about a decade ago (3.79×10^{-43} cm^2). This discrepancy is due to the significant contribution of GT transition strengths, which was previously not taken into account.

Based on ^{40}Ti β-decay measurement of present work and that of Trinder *et al.* [14], we derived a recommended value of $14.3(3)\times10^{-43}$ cm^2 for the neutrino absorption cross-sections of ^{40}Ar. This result represents the weighted average of the experimental values of $13.8(6)\times10^{-43}$ and $14.5(4)\times10^{-43}$ cm^2 (see Table VI). The averaging procedure was based on weights deduced from the uncertainties of the individual experimental results. This approach, which neglects the fact that we used a common Q_{EC} value (11466(13) keV, see Sect. III.E), is probably justified as the latter has only a minor inflence on the individual uncertainties.

The recommended neutrino absorption cross-section, together with the solar neutrino flux according to [30], yields a recommended value of the neutrino induced event rates for the ICARUS detector of $9.4\pm0.2(\text{stat.})^{+1.3}_{-1.6}(\text{syst.})$ SNU.

V. SUMMARY AND OUTLOOK

The β-decay of ^{40}Ti and ^{41}Ti was investigated by detecting β-delayed proton and γ-rays. For both nuclei, the half-lives were measured and the β-transition strengths were deduced.

From the non-observation of β-delayed γ-rays for ^{40}Ti and ^{41}Ti, and from the integrated b_β values of 101(5) % and 104(5) %, respectively, we conclude that, within the sensitivity of the present experiment, β-delayed proton emission is the only disintegration mode in both cases. The occurrence of a β-delayed proton branching ratio close to 100 % for ^{40}Ti and ^{41}Ti is due to two effects. On the one hand, the β-decay of ^{40}Ti (0^+) and ^{41}Ti ($3/2^+$) to the ground state of ^{40}Sc (1^-) and ^{41}Sc ($7/2^-$), respectively, is forbidden. On the other hand, *all* excited levels of ^{40}Sc and ^{41}Sc, populated in β-decay, are unbound against proton emission. This feature reflects the fact that, as the proton emitting nucleus (Sc) has odd-Z

and its proton daughter (Ca) represents a proton shell closure (Z=20), the proton separation energies for ^{40}Sc and ^{41}Sc are unusually low (539(4) keV and 1085.07(9)keV, respectively [10]). If one extends such simple considerations from ^{40}Ti to heavier nuclei of the T_z = -2, A = 4n series, one would expect ^{56}Zn to also be a pure β-delayed proton emitter. The corresponding extension of the T_z = -3/2, A = 4n+1 series beyond ^{41}Ti explains the observation of β-delayed protons form ^{57}Zn [31].

The comparison with the shell-model prediction shows that the quenching factor of 0.775 in the GT operator is adequate for describing the total $B(GT)$ strength of ^{40}Ti. Further improvement is needed, however, to account for the discrepancy between experiment and theory in the *shape* of the $B(GT)$ distribution. Comparing the present results for ^{41}Ti with shell-model calculation reveals a quenching factor of 0.93(3), i.e. higher than that of ^{40}Ti.

The experimental $B(GT)$ data for ^{40}Ti were used to calculate the neutrino absorption cross-section for the ICARUS detector as $9.1\pm0.2(\text{stat.})^{+1.3}_{-1.6}(\text{syst.})$ SNU. The major part of the (systematical) uncertainty is due to the limited knowledge of the solar-neutrino flux. We also note that the Q_{EC} value, used in this evaluation, does not stem from experiment, but from an IMME analysis.

An improvement of the ^{40}Ti data obtained in this work could in principle be realized by using sources prepared by an isotope separator on line. This method would yield superior proton energy resolution compared to the present work. Furthermore, measurements could be extended to *higher proton energies* by choosing the adequate detector thickness without the line-shape limitations related to deep implantation. However, it is far from being obvious that ^{40}Ti sources of sufficient strength and purity can be produced at an isotope separator online.

ACKNOWLEDGMENTS

The authors would like to thank B.D. Anderson for making the ^{40}Ar(p,n)^{40}K data available prior to publication. WL would like to acknowledge support by the Deutscher Akademis-

cher Austauschdienst and the Hongkong Qiushi Science Foundation. MH would like to thank the Alexander von Humboldt-Foundation for support. This work was supported by the European Union under Contract No. ERBFMGE-CT95-0083.

REFERENCES

[1] ICARUS Collaboration, ICARUS II Proposal, LNGS Report 95/99-I(1993), see also *http://www.aquila.infn.it:80/icarus/main.html.*

[2] J.N. Bahcall *et al.*, Phys. Lett. B178 (1986) 324.

[3] B.A. Brown *et al.*, At. Data Nucl. Data s 33 (1985) 347.

[4] E.G. Adelberger *et al.*, Phys. Rev. Lett. 67 (1991) 3658.

[5] W. Trinder *et al.*, Phys. Lett. B348 (1995) 331.

[6] W. Trinder *et al.*, Phys. Lett. B349 (1995) 267.

[7] W. Trinder *et al.*, Nucl. Phys. A620 (1997) 191.

[8] W.E. Ormand *et al.*, Nucl. Phys. A491 (1989) 1.

[9] B.A. Brown, Phys. Rev. Lett. 69 (1992) 1034.

[10] G. Audi *et al.*, Nucl. Phys. A624 (1997) 1.

[11] B. D. Anderson *et al.*, Phys. Rev. C54 (1996) 602.

[12] C. Détraz *et al.*, Nucl. Phys. A519 (1990) 529.

[13] W. Liu *et al.*, Z. Phys. A386 (1997)1.

[14] W. Trinder *et al.*, Phys. Lett. B 415 (1997) 211.

[15] H. Geissel *et al.*, Nucl. Instr. Meth. B70 (1992) 286.

[16] V. Metag *et al.*, Comments Nucl. Part. Phys. 16 (1986) 213.

[17] A. Piechaczek, Ph.D. thesis, Technische Hochschule Darmstadt 1991.

[18] A. Honkanen *et al.*, Nucl. Phys. A621(1997) 689.

[19] W. Trinder, Ph.D. thesis, Universität Frankfurt a.M. 1995.

[20] C. Scheidenberger, computer code ATIMA.

[21] W. Trinder, computer code EFFPROT.

[22] K. Sümmerer *et al.*, Phys. Rev. C42 (1990) 2546.

[23] R.G. Sextro *et al.*, Nucl. Phys. A234 (1974)130.

[24] Z. Y. Zhou *et al.*, Phys. Rev. C31 (1985) 1941.

[25] L. Faux *et al.*, Nucl. Phys. A602 (1996)167.

[26] B. D. Anderson, private communication

[27] W.E. Ormand *et al.*, Phys. Lett. B345 (1995) 343.

[28] N. I. Kaloskamis *et al.*, Phys. Rev. C55 (1997) 630.

[29] D. J. Vieira, Ph.D. thesis, LBL-7161 (1978).

[30] J.N. Bahcall, Rev. Mod. Phys. 67(1995)781.

[31] D. J. Vieira, Phys. Lett. 60B (1976) 261.

FIGURES

FIG. 1. Sketch of the detector set-up at the intermediate and final focal plane of the FRS, see text for details.

FIG. 2. Energy-loss vs. mass-to-charge scatter plot for the ^{40}Ti data set. The location of ^{40}Ti and ^{38}Ca ions is indicated. The ^{40}Ti events, used in the data evaluation, are marked by a frame.

FIG. 3. Range profile of the ^{40}Ti ions implanted into the silicon detectors. The thickness of each silicon detector was 300 μm. The experimental data are shown as a histogram with a Gaussian fit superimposed.

FIG. 4. Energy spectrum of β-delayed protons measured for the decay of ^{40}Ti.

FIG. 5. Energy spectrum of β-delayed protons measured for the decay of ^{41}Ti.

FIG. 6. Section of the energy spectrum of β-delayed protons measured for the decay of ^{40}Ti. The fit of the 3731 keV line is shown as a dashed curve. The individual peaks are marked according to Table I.

FIG. 7. Proton energy spectrum recorded in one of the silicon detectors under the restriction that ^{40}Ti ions are implanted into the central 100 μm thick silicon layer.

FIG. 8. Full-energy detection efficiency deduced from experimental data (full points) and from a Monte-Carlo simulation (solid line).

FIG. 9. Energy-loss versus residual energy scatter plot of ^{40}Ti event observed after the energy degrader in the final focal plane of the FRS. The cluster of events, corresponding to titanium ions, is marked.

FIG. 10. Scatter plot of the proton-γ coincidence data obtained for ^{40}Ti. The coincidence events between 1322 keV proton and 2469 keV γ-ray are marked by a frame.

FIG. 11. Gamma-ray spectrum measured in coincidence with 1322 keV proton events (open histogram), compared to that obtained in coincidence with 2167 keV proton events (hatched histogram). In the latter case, the intensity was scaled to match the number of counts in the 511 keV peak.

FIG. 12. Experimental time spectrum for ^{40}Ti (histogram) and result obtained from a one-component fit (solid line).

FIG. 13. Comparison of Gamow-Teller strength distributions for the ^{40}Ti decay obtained from the present work, another recent β-decay experiment, a ^{40}Ar(p,n)^{40}K measurement, and a shell-model calculation.

FIG. 14. Comparison of Gamow-Teller strength distributions for the ^{41}Ti β-decay, obtained from the present work and the work of Honkanen *et al.*.

TABLES

TABLE I. Energies E_p and branching ratios b_p of β-delayed protons for the decay of ^{40}Ti

	This work		Trinder *et al.*	
Peak no.	E_p (keV)	b_p (%)	E_p (keV)	b_p (%)
1	242(40)[a]	1.32(40)		
2	400(30)[a]	0.70(30)		
3	759(30)[a]	0.77(43)	709(25)	0.34(10)
4	951(43)[b]	0.80(32)		
5	1157(30)	0.77(42)	1105(26)	0.31(11)
6	1322(25)	4.35(82)	1322(9)	3.46(25)
7	1580(20)[a]	0.40(20)	1574(28)	0.45(12)
8	1705(10)	22.5(21)	1698(9)	24.9(70)
9	1992(20)[a]	0.95(43)	1957(79)	1.3(20)
10	2167(10)	28.5(19)	2159(10)	29.4(14)
11	2366(20)	0.60(18)	2355(35)	0.86(22)
12	2518(23)	1.01(56)	2481(26)	1.6(30)
13	2609(30)	1.05(42)		
14	2733(20)	1.6(11)	2708(31)	1.6(30)
15	2907(20)	0.69(28)	2902(31)	1.3(30)
16	3045(20)	1.43(78)	3046(23)	1.8(30)
17	3158(27)	3.4(16)	3153(20)	2.9(40)
18	3407(44)	0.57(30)	3128(35)	1.1(20)
19	3632(23)	1.09(27)	3633(21)	0.99(18)
20	3731(10)	22.8(19)	3733(12)	21.8(15)
21	3972(50)	1.40(42)	3890(33)	1.4(30)
22	4137(30)	1.27(53)	4015(32)	1.5(40)
23	4347(37)	0.97(40)	4353(99)	2(1)

24	4481(44)	0.73(22)		
25	4702(30)	0.55(21)		
26	4909(20)	0.16(10)	4951(60)	0.63(20)
27	5107(30)	0.41(30)		
28	5213(40)	0.30(12)		
29	5418(30)	0.18(10)	5308(33)	0.68(20)
30	5740(30)	0.11(6)		

[a]Transition feeding the 2469 keV state in ^{39}Ca.

[b]Transition feeding the 3026 keV state in ^{39}Ca.

TABLE II. Energies and relative branching ratios (b_p^{rel}) of β-delayed protons observed for the decay of ^{41}Ti. The b_p^{rel} values were chosen for a comparison with the data given in Refs. [18,23,24]. The b_p^{rel} values from this work have to be multiplied by a factor 0.261 to yield absolute branching ratios b_p.

This work		Honkanen *et al.* [18]		Sextro *et al.* [23] and Zhou *et al.* [24]	
E_p (keV)	b_p^{rel}(%)	E_p (keV)	b_p^{rel}(%)	E_p (keV)	b_p^{rel}(%)
744(30)	4.3(14)	754(12)	1.1(5)		
976(30)	24.0(64)	986(2)	19.6(19)	1000(15)	38.6(24)
1272(35)[a]	5.0(15)			1248(15)	3.9(9)
1540(20)	20.8(21)	1542(2)	28.8(23)	1546(15)	21.6(7)
		1586(11)	4.0(9)		
1842(20)[a]	3.3(12)				
1987(30)[a]	5.2(13)	1981(12)	2.6(7)	1983(25)	3.1(6)
2111(21)[a]	3.3(7)			2063(30)	4.1(5)
2270(25)	21.0(57)	2270(3)	17.9(18)	2271(10)	26.1(9)
2440(20)	7.3(53)	2414(3)	8.3(12)	2409(20)	14.7(3)
2538(64)	2.5(5)				
2654(20)	7.3(32)	2650(12)	7.0(11)	2662(20)	8.1(8)
2817(23)	5.2(16)	2796(14)	2.1(6)	2814(15)	4.9(5)
3095(10)	67.3(73)	3080(5)	66.0(30)	3077(15)	60.3(38)
3295(20)	3.5(18)	3139(12)	2.8(6)	3148(20)	4.0(11)
		3330(13)	2.2(6)	3339(30)	2.3(4)
3452(35)	3.7(19)	3480(12)	2.1(6)	3487(20)	2.8(4)
3569(20)	5.1(21)	3598(6)	7.2(10)	3605(15)	9.7(4)
3647(25)	5.3(20)	3691(5)	17.8(16)	3590(15)	15.5(8)
3749(18)	39.0(40)	3749(5)	29.2(21)	3749(10)	31.0(20)
3857(20)	2.0(11)	3837(9)	3.4(8)	3836(25)	2.4(2)

4025(20)	2.0(7)	3888(11)	3.2(8)	3904(25)	1.5(2)
4192(10)	12.8(27)	4189(6)	13.1(14)	4187(15)	15.4(5)
		4298(13)	1.3(5)		
4376(20)	9.2(21)	4381(8)	6.0(9)	4379(15)	7.2(4)
4486(30)	4.9(20)	4567(8)	2.2(3)	4564(20)	2.2(3)
4625(33)	6.3(41)	4639(5)	19.1(17)	4638(10)	22.1(7)
		4684(11)	4.1(8)		
4727(16)	107(11)[b]	4736(5)	100	4734(4)	100
				4832(25)	3.0(3)
4883(30)	2.4(12)			4876(20)	3.4(4)
4976(20)	3.6(17)	4950	14(5)	4925(20)	2.9(3)
5093(20)	2.1(15)			5177(30)	1.5(3)
5219(20)	2.6(5)				
5364(30)	1.5(8)				
5451(20)	2.4(5)				
5658(20)	3.0(15)			5595(15)	0.26(3)
5736(20)	1.1(4)			5715(15)	0.36(6)
5889(47)	0.8(2)			5950(20)	0.40(3)
6082(30)	0.6(2)			6125(20)	0.29(2)
6359(30)	0.4(1)			6380(50)	0.20(3)
6725(30)	0.3(1)			6650(50)	0.20(2)

[a]Transition feeding the 3904 keV state in ^{40}Ca.

[b]Due to limited resolution of this work, the neighbouring 4684 and 4832 keV peaks, observed by Honkanen *et al.* and Sextro *et al.*, respectively, remain unresolved.

TABLE III. Energies of excited levels in ^{40}Sc, β-branching ratios, and β-transition strengths for ^{40}Ti decay, and ^{40}Ar neutrino capture cross-sections deduced from the present data, in comparison with the results from other work. p_0, p_1, p_2 denote proton transitions to the ground state, first excited state (2469 keV) and second excited state (3026 keV) of ^{39}Ca.

		This work				Trinder *et al.* [14]		(p,n) data [26]	
E_x(^{40}Sc) (keV)	Decay mode	b_β (%)	$B(F)$ $+B(GT)$	E_x (^{40}K) (keV)	σ_ν (10^{-43}cm^2)	E_x (^{40}Sc) (keV)	$B(F)$ $+B(GT)$	E_x (^{40}K) (keV)	$B(F)$ $+B(GT)$
2287(10)	p_0	22.5(21)	0.83(8)	2290	2.82(26)	2281(9)	0.96(3)	2280	1.23(24)
2761(10)	p_0	28.5(19)	1.40(10)	2730	3.80(26)	2753(11)	1.50(7)	2730	1.05(21)
2966(20)	p_0	0.60(18)	0.03(1)		0.080(24)	2955(35)	0.05(1)		
3121(23)	p_0	1.01(56)	0.06(3)	3110	0.138(77)	3084(26)	0.10(2)		
3235(25)	p_0,p_1	2.37(58)	0.16(4)		0.324(80)				
3342(20)	p_0	1.6(11)	0.11(8)	3150	0.21(14)	3317(31)	0.11(2)	3376	0.09(2)
3418(30)	p_1	0.70(30)	0.05(2)		0.097(42)				
3521(20)	p_0	0.69(28)	0.06(2)		0.096(39)	3515(31)	0.11(2)		
3662(20)	p_0	1.43(78)	0.13(7)		0.20(11)	3664(23)	0.16(3)		
3782(20)	p_0,p_1	4.2(17)	0.40(16)	3739	0.61(24)	3758(20)	0.32(5)	3830	0.28(6)
4033(44)	p_0	0.57(30)	0.07(4)		0.081(44)	4055(35)	0.14(3)		
4194(30)	p_1	0.77(42)	0.10(6)		0.111(61)	4141(26)	0.04(1)		
4264(23)	p_0	1.09(27)	0.15(4)		0.158(39)	4265(22)	0.14(3)		
4365(10)	p_0,p_1	27.1(21)	4.01(31)	4381	3.87(30)	4365(8)	3.90(25)	4380	0.71(35)[a]
4540(43)	p_2	0.80(32)	0.14(5)		0.116(46)	4528(33)	0.24(6)		
4628(20)	p_0,p_1	1.80(47)	0.33(9)		0.262(68)	4637(29)	0.38(8)		
4782(30)	p_0	1.27(53)	0.26(11)	4789	0.183(77)			4760	0.30(6)
4997(36)	p_0	0.97(40)	0.24(10)		0.140(58)				
5051(20)	p_1	0.95(43)	0.25(11)		0.137(63)	5003(99)	0.90(30)		
5135(43)	p_0	0.73(22)	0.20(6)		0.105(32)			5160	0.33(7)

5362(30)	p_0	0.55(21)	0.19(7)	0.077(30)				
5574(20)	p_0	0.16(10)	0.07(4)	0.022(14)	5617(61)	0.28(9)		
5777(30)	p_0	0.41(30)	0.21(15)	0.054(40)			5700	0.07(1)
5886(40)	p_0	0.30(12)	0.17(7)	0.038(15)				
6126(30)	p_0	0.18(10)	0.13(7)	0.022(13)	5983(33)	0.44(13)	6110	0.26(5)
6426(30)	p_0	0.11(6)	0.11(6)	0.012(6)				

[a]There appears to be some significant GT strength unresolved from the 0^+, IAS. Fermi strength [26].

TABLE IV. Energies of excited levels in ^{41}Sc, β-branching ratios, β-transition strengths deduced from this work, in comparison with other works. p_0, p_1 denote proton transitions to the ground state, first excited state (3904 keV) of ^{40}Ca.

This work				Honkanen *et al.* [18]	
$E_x(^{41}\mathrm{Sc})$ (keV)[a]	decay	b_β (%)	$B(F)+B(GT)$	E_x (^{41}Sc) (keV)	$B(F)+B(GT)$
2095.9(5)	p_0	6.3(17)	0.06(2)	2095.9(5)	0.057(12)
2666.60(7)	p_0	5.4(6)	0.07(1)	2666.60(7)	0.108(21)
				2719.12(9)	0.016(5)
3411.4(4)	p_0	5.5(15)	0.11(3)	3411.4(4)	0.097(12)
3562.6(3)	p_0	1.9(14)	0.04(3)	3562.6(3)	0.049(9)
3687(20)	p_0	0.7(1)	0.014(3)		
3780.6(2)	p_0	1.9(8)	0.05(2)	3780.6(2)	0.047(9)
3971(15)	p_0	1.4(4)	0.04(1)	3951(14)	0.015(5)
4245(4)	p_0	17.6(19)	0.58(7)	4245(4)	0.580(50)
				4328(3)	0.026(7)
4502(5)	p_0	0.9(5)	0.04(2)	4502(5)	0.023(7)
4661(2)	p_0	1.0(5)	0.04(2)	4644(5)	0.024(7)
4777(5)	p_0	1.3(6)	0.06(3)	4777(5)	0.090(15)
4869(4)	p_0	1.4(5)	0.07(3)	4869(4)	0.240(30)
4947(5)	p_0	10.2(10)	0.53(6)	4928(5)	0.400(40)
5023(5)	p_0	0.5(3)	0.03(2)	5023(5)	0.050(13)
				5084(5)	0.049(13)
5210(20)	p_0	0.5(2)	0.03(1)		
5375(5)	p_0	3.3(7)	0.23(5)	5375(5)	0.250(30)
				5193(5)	0.027(11)
5576(4)	p_0	2.4(6)	0.19(5)	5576(4)	0.130(30)
5683(30)	p_0	1.3(5)	0.11(5)		

5774(4)	p_1	1.1(4)	0.11(3)	5774(4)	0.110(30)
5863(5)	p_0	1.6(11)	0.16(11)	5840(5)	0.510(60)
5886(12)	p_0	0.9(5)[b]	0.09(5)	5886(12)	0.110(30)
5939(4)	p_0	26.1(29)	2.77(34)	5939(4)	2.87(22)
6038(25)	p_0	0.9(5)[b]	0.10(6)	6038(25)	0.81(11)[c]
6090(30)	p_0	0.6(3)	0.08(4)	6083(20)	0.096(13)
6185(20)	p_0	0.9(5)	0.12(6)	6133(20)	0.085(11)
6299(20)	p_0,p_1	1.9(6)	0.26(8)	6391(30)	0.054(13)
6435(20)	p_0	0.7(1)	0.11(2)	6468(12)	0.120(40)
6583(30)	p_0	0.4(2)	0.07(4)		
6672(20)	p_0	0.6(1)	0.12(3)		
6881(14)	$p_{0,1}$	1.7(5)	0.39(12)	6820(15)	0.016(2)
6964(20)	p_0	0.3(1)	0.07(3)	6942(15)	0.024(3)
7026(30)	p_1	1.4(3)	0.37(9)		
7137(26)	p_0,p_1	1.1(2)	0.33(6)	7180(20)	0.034(5)
7319(30)	p_0	0.17(5)	0.06(2)	7360(20)	0.029(3)
7603(30)	p_0	0.11(2)	0.05(1)	7630(50)	0.027(5)
7978(30)	p_0	0.07(3)	0.05(2)	7900(50)	0.037(5)

[a]Adopted best values either from this work or from Ref. [18]

[b]Decomposed using the information from Ref. [18]

[c]Most probably misprinted in Ref. [18], was calculated to be 0.081(11) according to the b_3 value in Ref. [18].

TABLE V. Summary of measured half-lives in ms for ^{40}Ti and ^{41}Ti.

	This work	Détraz *et al.* [12]	Trinder *et al.* [14]	
^{40}Ti	54(2)	56^{+18}_{-12}	51.7(6)	
	This work	Sextro *et al.* [23]	Faux *et al.* [25]	Trinder *et al.* [14]
^{41}Ti	82(3)	80(2)	81(4)	80.1(9)

TABLE VI. Comparison of ^{40}Ar neutrino absorption cross-sections and neutrino induced event rates for ICARUS detector.

	Cross sections (10^{-43} cm^2)	Solar neutrino flux (10^6 cm^2)	Event rates (SNU)
This work. β-decay data	13.8(6)	$6.6^{+0.9}_{-1.1}$ [30]	$9.1\pm0.4(\text{stat.})^{+1.3}_{-1.6}(\text{syst.})$
Liu *et al.* [13]	-	5.8(21) [2]	6.8(26)
Trinder*et al.* [14]	14.5(4)	$6.6^{+0.9}_{-1.1}$ [30]	$9.6^{+1.4}_{-1.7}$
This work. (p,n) data[a]	11.9(10)	$6.6^{+0.9}_{-1.1}$ [30]	$7.9\pm0.7(\text{stat.})^{+1.2}_{-1.5}(\text{stat.})$
Ormand *et al.* [27]	11.5(7)	5.8(21) [2]	6.7(25)
Bahcall *et al.* [2]	3.79	-	-
Recommended value	14.3(3)[b]	$6.6^{+0.9}_{-1.1}$ [30]	$9.4\pm0.2(\text{stat.})^{+1.3}_{-1.6}(\text{syst.})$

[a]Calculated using the $B(GT)$ values from Ref. [26] and the $B(F)$ value from this work.

[b]Weighted average of the results form this work and those form Trinder *et al.* [14].

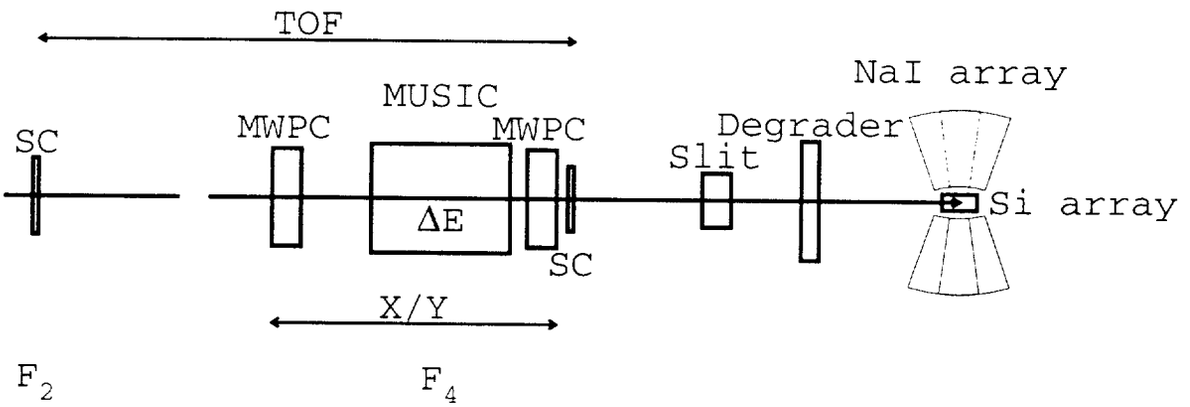
TOF
NaI array
MUSIC
MWPC
MWPC
Degrader
SC
Slit
ΔE
Si array
SC
X/Y
F2
F4

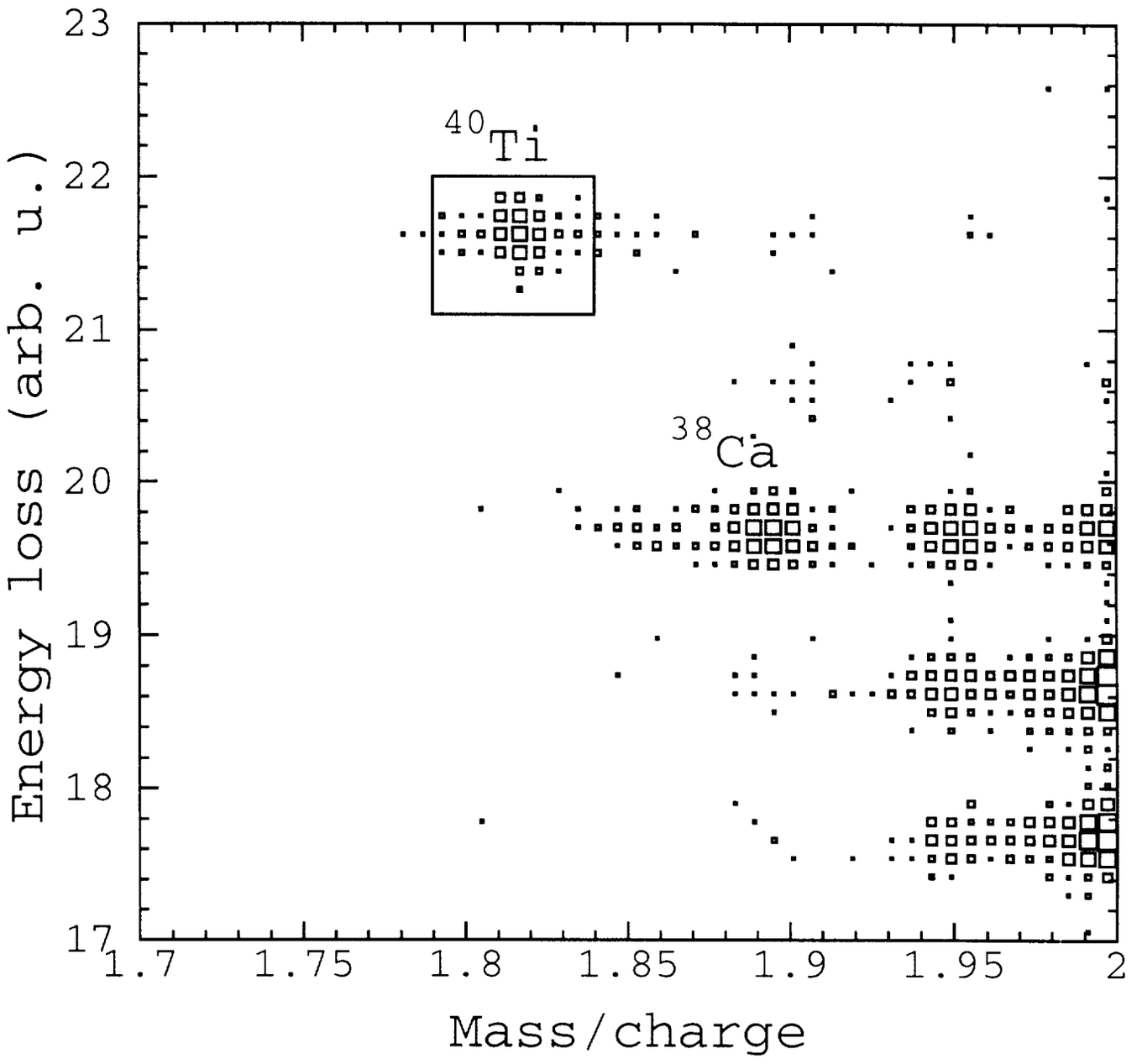
Energy loss (arb. u.)
23
22
21
20
19
18
17
1.7
1.75
1.8
1.85
1.9
1.95
2
Mass/charge
40Ti
38Ca

Fig. 2

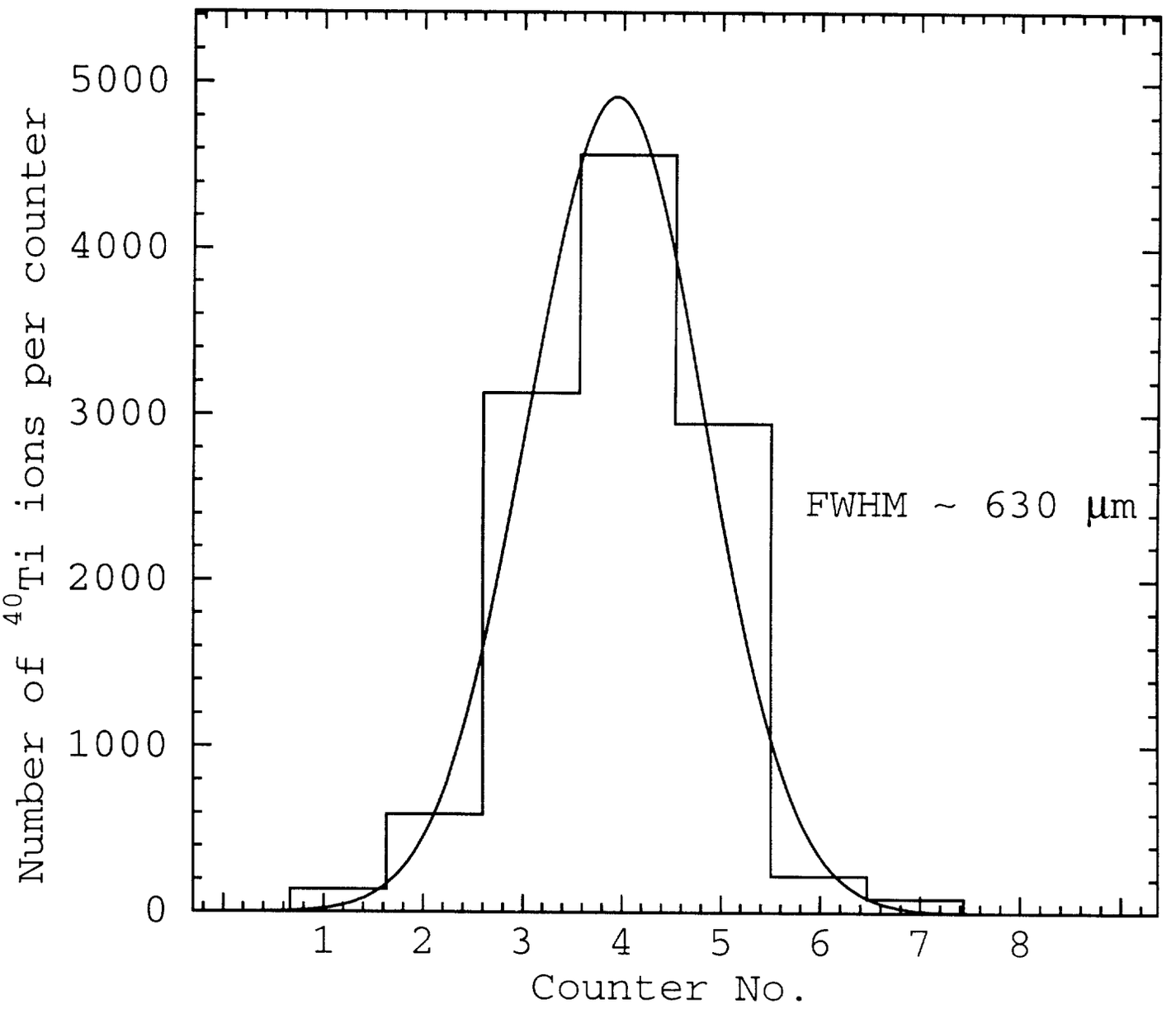
Number of ^{40}Ti ions per counter
5000
4000
3000
2000
1000
0
1
2
3
4
5
6
7
8
Counter No.
FWHM ~ 630 μm

Fig. 5

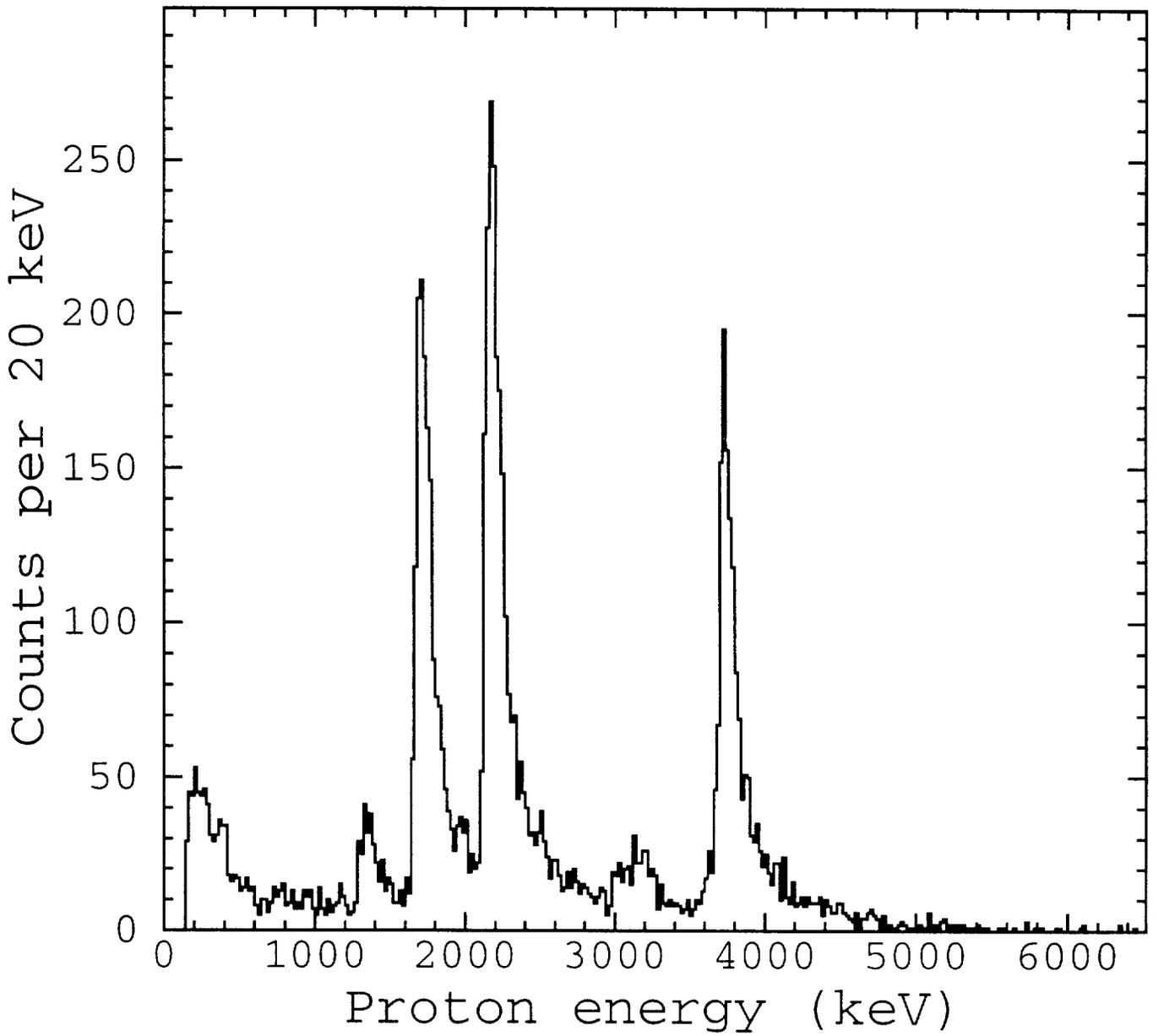
Counts per 20 keV
0
50
100
150
200
250
0
1000
2000
3000
4000
5000
6000
Proton energy (keV)

Fig 4

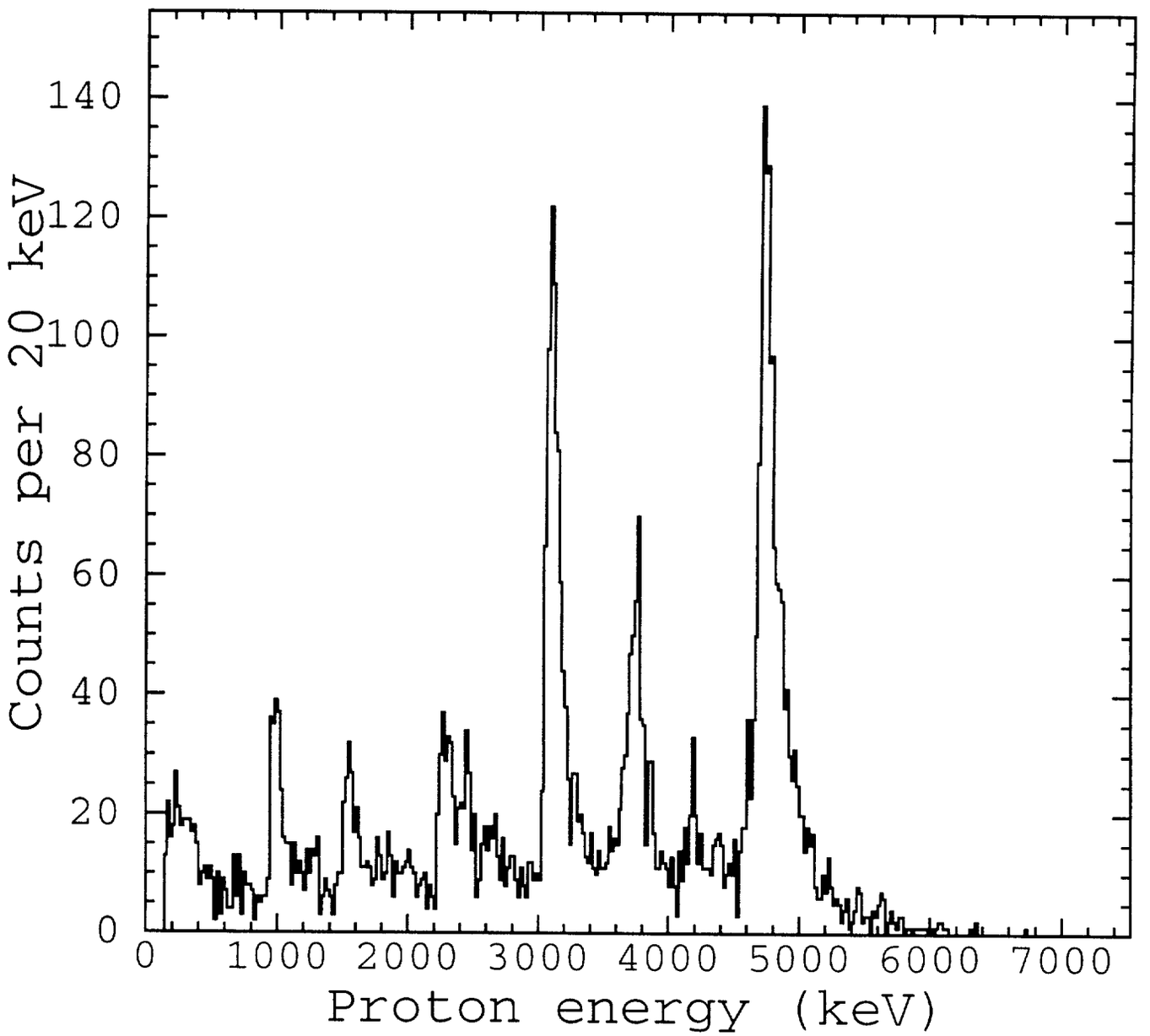
Counts per 20 keV
0
20
40
60
80
100
120
140
0
1000
2000
3000
4000
5000
6000
7000
Proton energy (keV)

Fig. 5

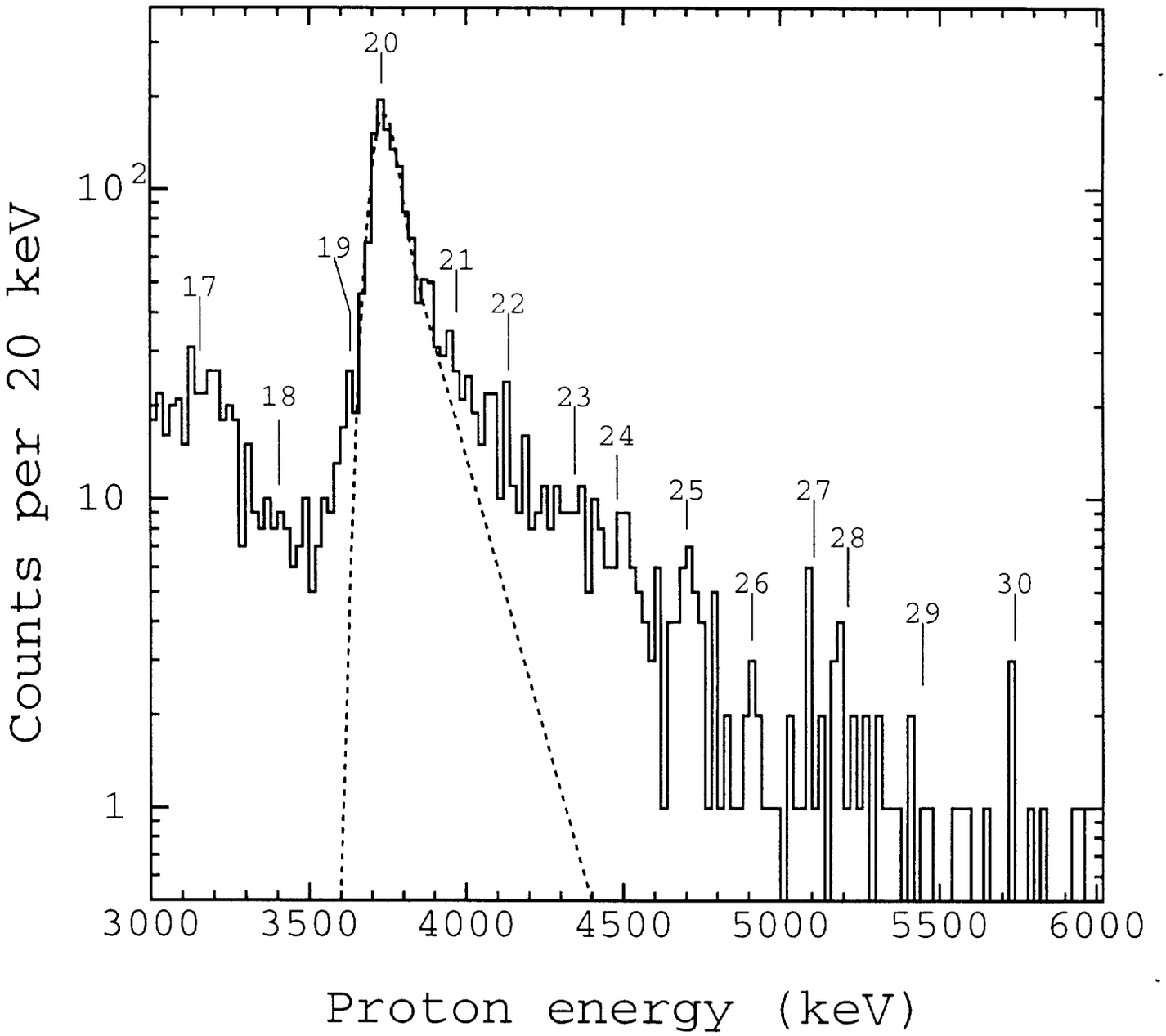
Counts per 20 keV
10 2
10
1
3000
3500
4000
4500
5000
5500
6000
Proton energy (keV)
17
18
19
20
21
22
23
24
25
26
27
28
29
30

Fig. 6

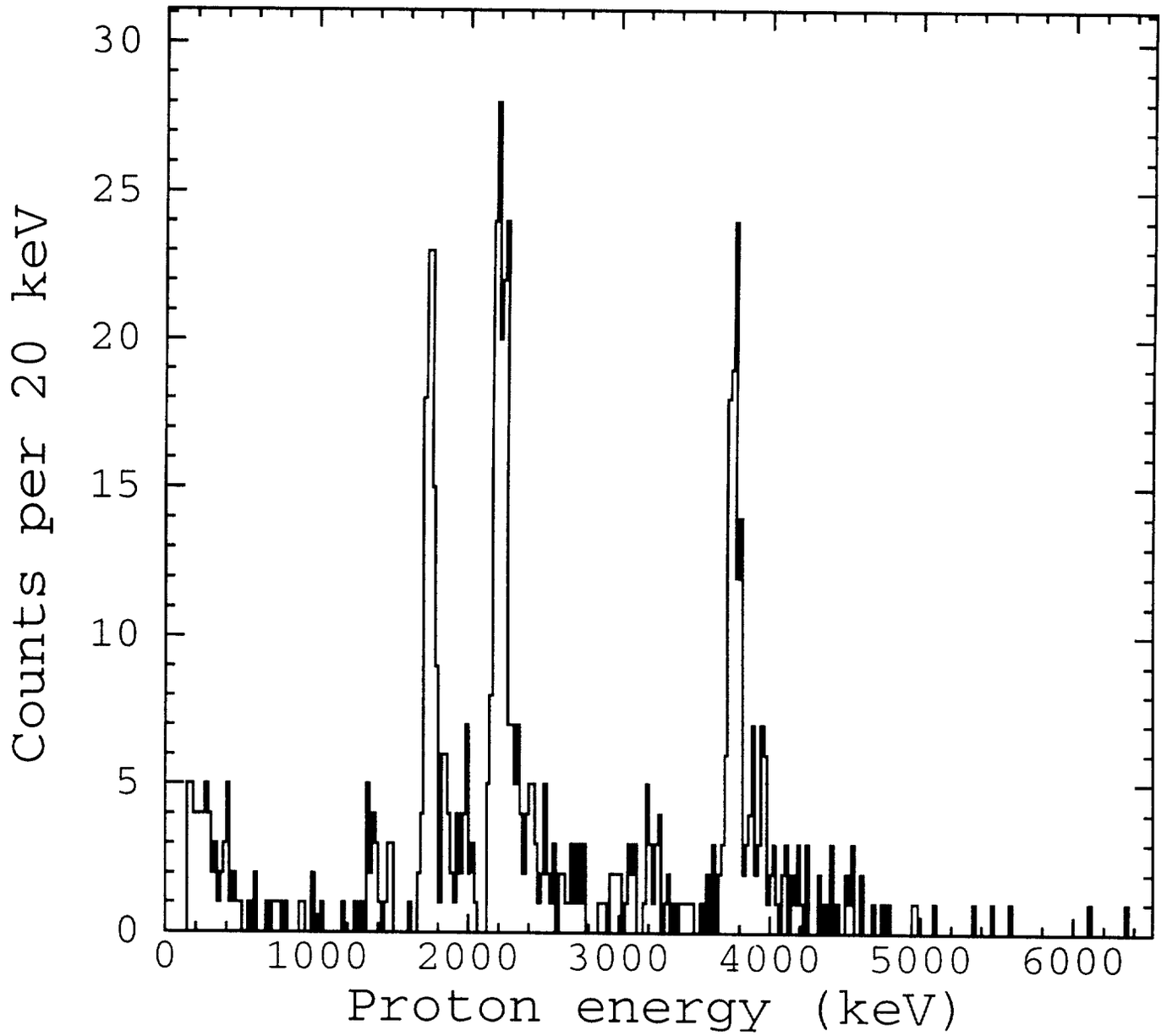
Counts per 20 keV
Proton energy (keV)
0
5
10
15
20
25
30
0
1000
2000
3000
4000
5000
6000

F-27

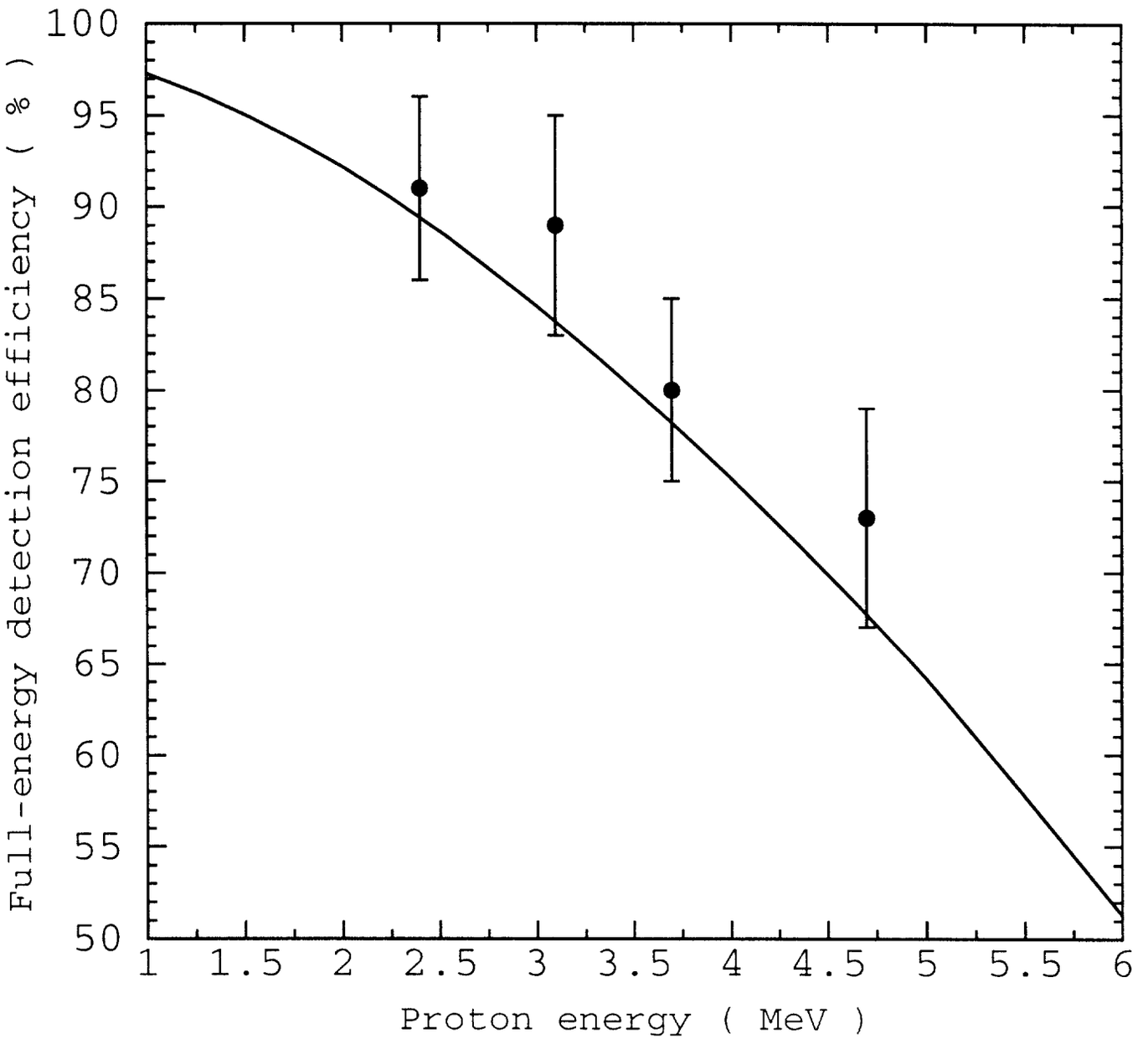
Full-energy detection efficiency (%)
100
95
90
85
80
75
70
65
60
55
50
1
1.5
2
2.5
3
3.5
4
4.5
5
5.5
6
Proton energy (MeV)

F 2.2

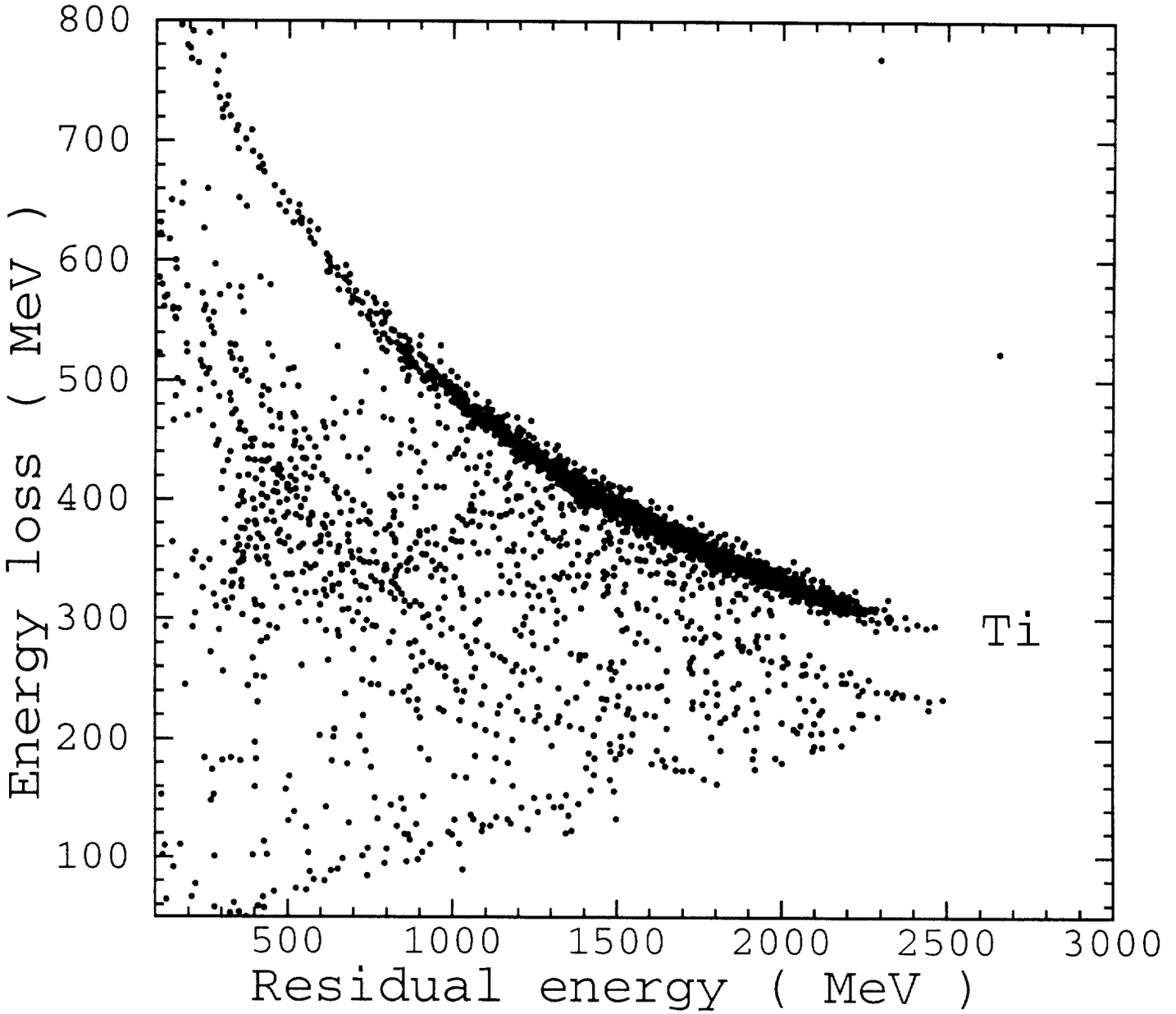
800
700
600
500
400
300
200
100
Energy loss (MeV)
500
1000
1500
2000
2500
3000
Residual energy (MeV)
Ti

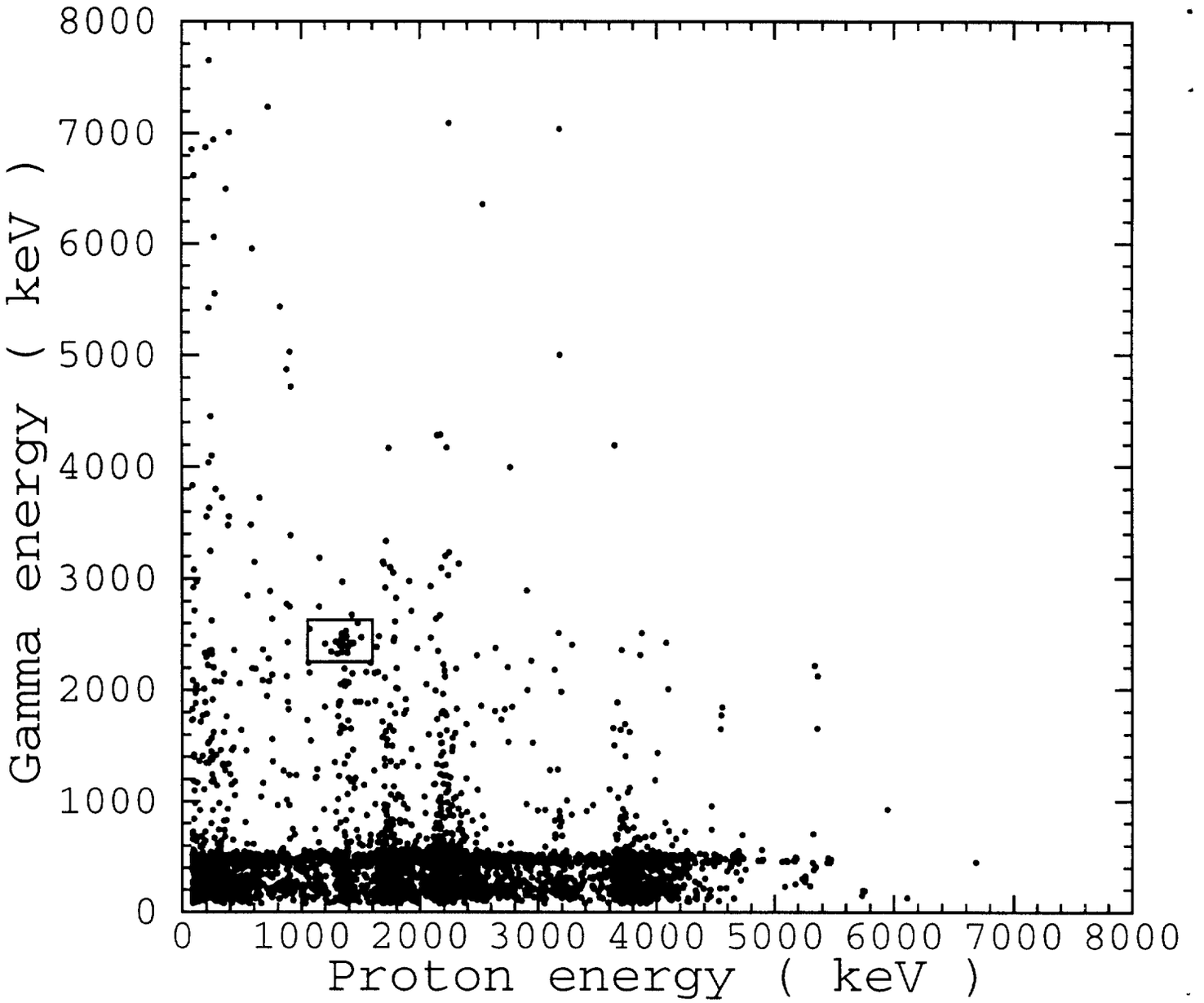
Gamma energy (keV)
Proton energy (keV)
0
1000
2000
3000
4000
5000
6000
7000
8000

Fig. 10

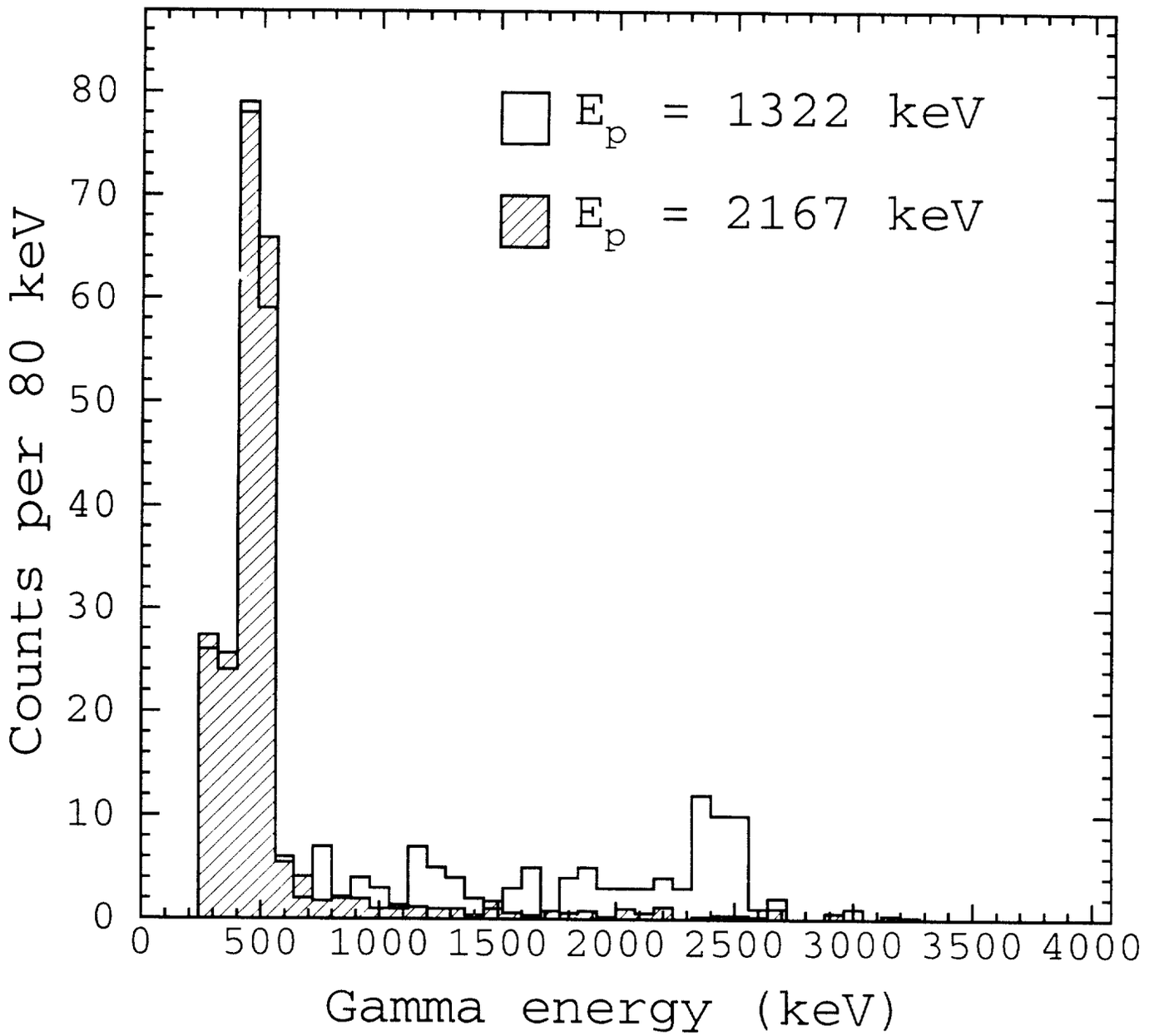
E_p = 1322 keV
E_p = 2167 keV
Counts per 80 keV
0
10
20
30
40
50
60
70
80
0
500
1000
1500
2000
2500
3000
3500
4000
Gamma energy (keV)

Fig. 11

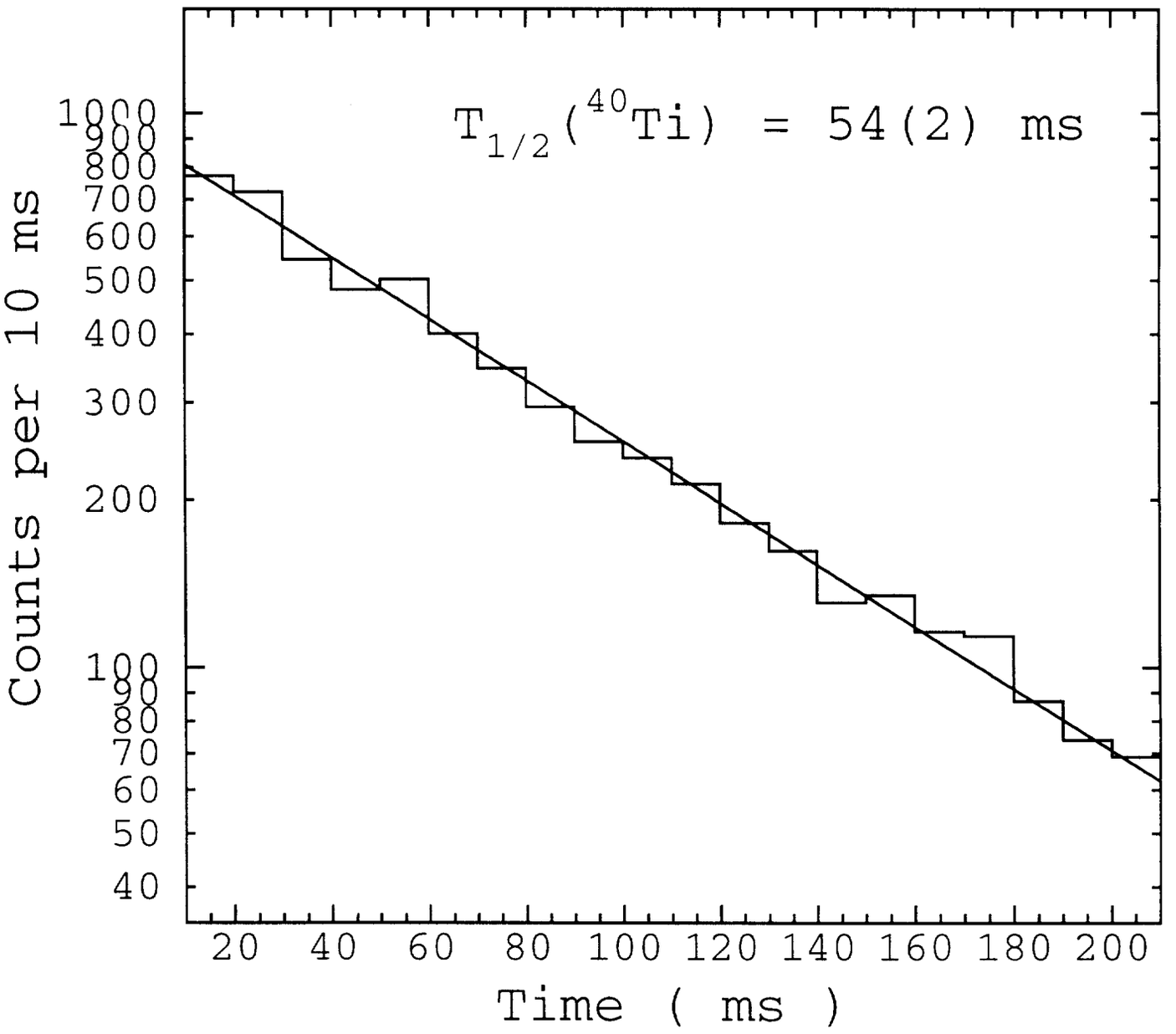
$T_{1/2}(^{40}Ti)$ = 54(2) ms
Counts per 10 ms
1000
900
800
700
600
500
400
300
200
100
90
80
70
60
50
40
20 40 60 80 100 120 140 160 180 200
Time (ms)

Fig. 12

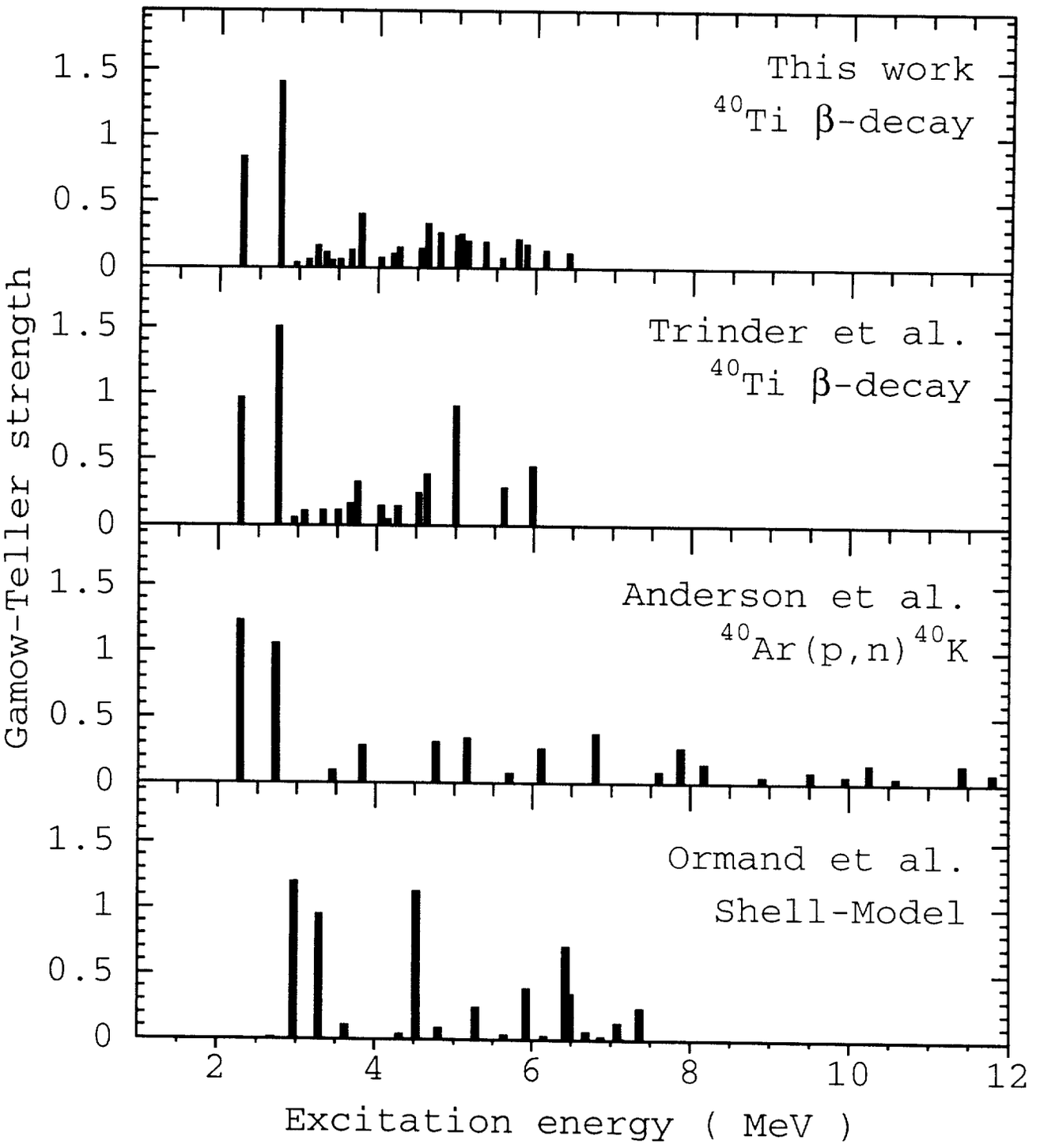
This work
^{40}Ti β-decay
Trinder et al.
^{40}Ti β-decay
Anderson et al.
^{40}Ar(p,n)^{40}K
Ormand et al.
Shell-Model
Gamow-Teller strength
Excitation energy (MeV)
0
0.5
1
1.5
2
4
6
8
10
12

Fig. 3

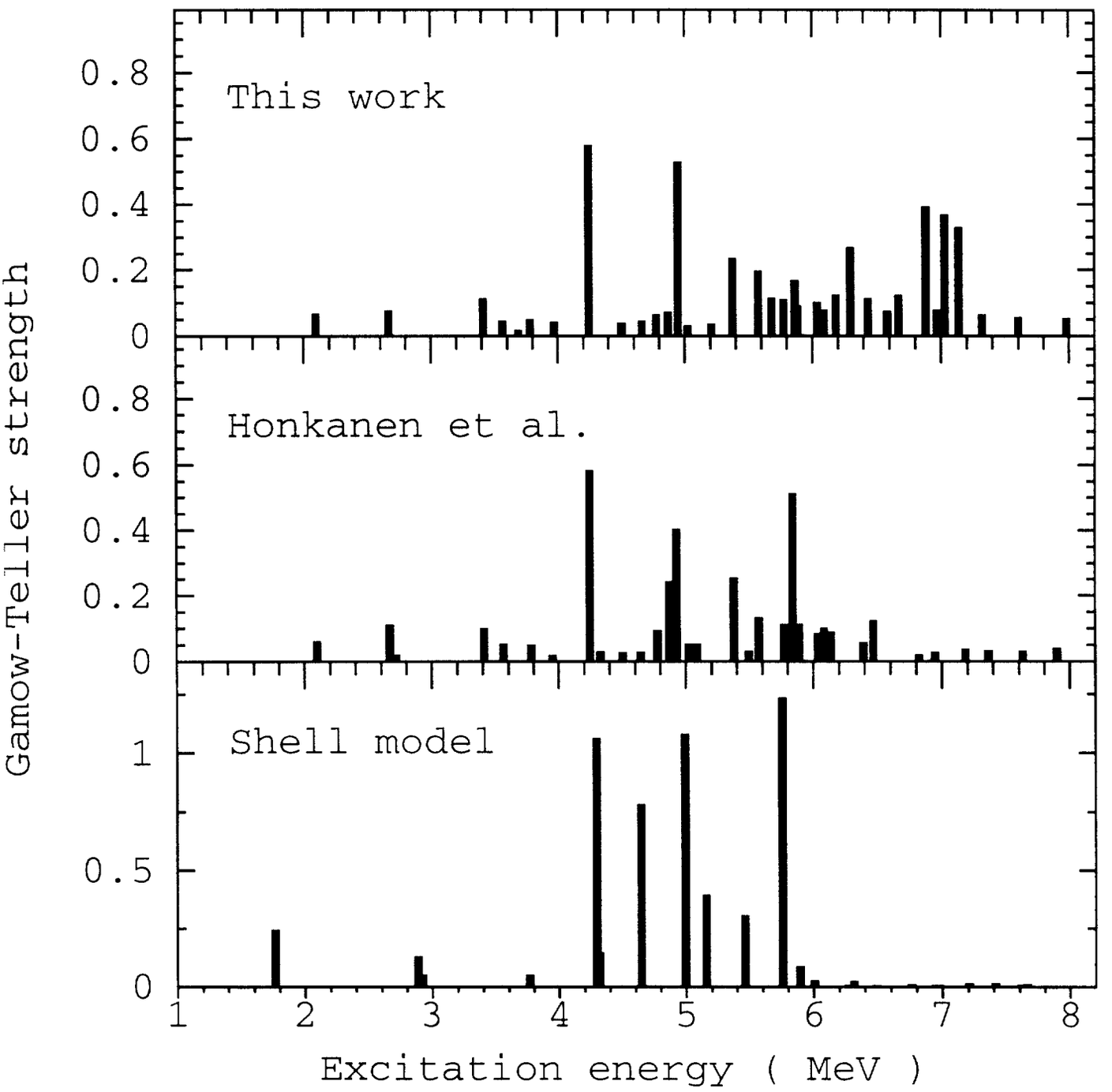
This work
Honkanen et al.
Shell model
Gamow-Teller strength
Excitation energy (MeV)
0.8
0.6
0.4
0.2
0
1
0.5
1
2
3
4
5
6
7
8